Modeling Piezoelectric Harvesting Materials in Road Traffic Applications

M. VÁZQUEZ-RODRÍGUEZ, F. J. JIMÉNEZ and J. DE FRUTOS

Abstract: - The method to obtain electrical equivalent models of piezoelectric materials used in energy harvesting road traffic environment is presented in this paper. The experimental results are processed in order to determine the optimal topological structure and technology of the semiconductor elements used in the input stage of the power harvesting system. The non regulated power supply model under variable current demand is also presented.

Key-Words: - Electric model, energy harvesting, piezoelectric material.

1 Introduction

Green and efficient energy generation is a challenge not only in transport, urban and industrial sectors, but also for microelectronic devices and electronic systems. Table 1 resumes several applications related with piezoelectric devices used as micro-power generators. Recently, powering sensor networks, monitoring devices and systems [17,18] related to civil infrastructures contribute the research in self-powered systems.

In order to obtain an electrical model of piezoelectric materials used as generators in road traffic applications a test bench [19] was developed to generate the electric signals produced by the piezoelectric materials in real traffic environment. In several cases is necessary associate the response of the material to an electronic circuit, to analyze generated power [20], use discontinuous conduction converters [21, 23] or adaptive circuits for remote applications [22]. In our case, using the characterization data collected with our road traffic test bench, the input stage electrical model of the energy harvesting system is obtained. This paper reviews the type and optimal topological structure of semiconductor elements to achieve optimal efficiency in that stage.

2 Piezoelectric Model under Road Traffic Stimulus

2.1 Test Bench

The test bench block diagram is presented in Fig. 1.

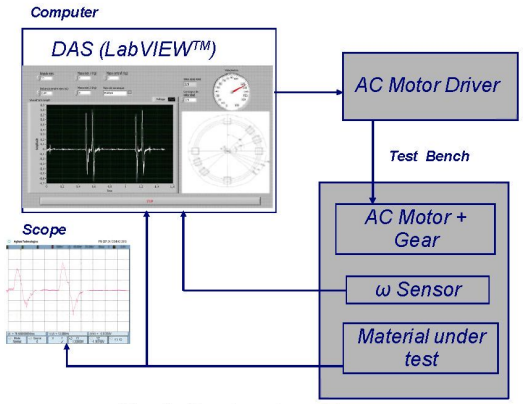

Fig. 1: Test bench architecture

In Fig. 2 it's presented a picture with a test in progress.

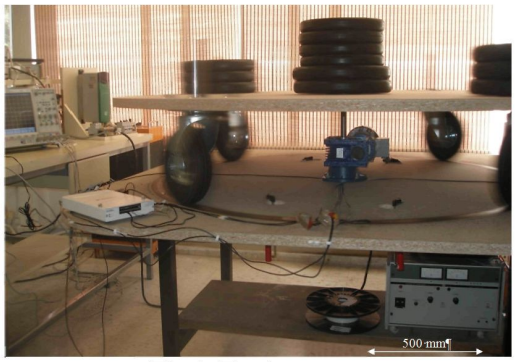

Fig. 2: Test in progress

The test bench performs the mechanical input to the materials, simulating continuous traffic conditions (like steady state traffic density). Table 2 presents a

test resume, at speeds between 14 and 116 km/h, and the peak voltage obtained in a piezoelectric cable.

TABLE 1
PIEZOELECTRIC POWER GENERATION

Material	Applications	Dimensions	Power (μW)	Power density (μW/cm3)	Voltage (V)	Resistance (kΩ)	Ref.
PZT Composites, d_{33} 39 MPa compress.	Composites			12000			1,2
PVF_2 Compress.	Windmill	500 μm*90 mm*70mm	2.4	0.76	1	400	3
BIMORPH PVDF. d_{31}	Shoe-mounted		1300		18	250	4
PZT DIMORPH, d31	Shoe-mounted		8400		64.8	500	4
PVDF bimorph. Windmill Rotor . 12 cantilevers bimorphs. Rotor d_{31} load	Windmill rotor	Each bimorph 60*20*0,5mm	10200	1420	6.8	4.6	5
PZT-5 A. LOAD MEMBRANE; BLOOD PRESSURE	Biomedical	Area 1cm^2 Thick. 9μm	2.3	2600			6
PZT rectangular structure	Knee Implant	1*1*1,8 cm^3	4800	890			7
Vibrant Transducer membrane	Low power sensors	Total radius: 20,5 mm (12,5mm PZT radius) , thick. 230 μm, Fastening thick.: 400 μm	1700	106	9	47	1,2
PZT thin layer. Cantilever generator	MEMS	(170*260) μm^2	1	740	2.2	5200	8
PZT thick layer, 80 Hz	MEMS	Layers of 20 μm	2		0.81	333	9
PZT, 1.5 MPa lateral pressure, 15 Hz	Wireless transmitter	Volume: 0.2 cm^3	1200	6000	9		10
PZT stacked generator(164 layers, 1 Hz , 250 N)	Muscle activation power	5*5*80 mm^3	690	345	19.3	540	1,2
Thin layer PZT membrane coupled with heat engine.	Hybrid	Surface: 3 mm^2 Thick: 3,4 μm	56	5.5 10^6	4		11
PZT Cymbal d33 load	Cymbal	Diameter: 29 mm Thickness: 1mm	39000	43900	400		12
PZT button (ignition) d33 load	Pulse generator	Diam:1.27 cm Thick: 1.3 mm	25 10^9	1.514 10^6	500	0.01	13
PMN-PT composites. d33 compressive load 40,4 MPa	Composite			22100			14
PZT between steel and brass. Stress cycles of 0.7 N, 590 Hz		0.51 cm^3	11000	21570	14.07	18	15
Piezoelectric nanowires Arrays and semiconductive ZnO	Biosensors and Electronic nanogenerators	Diameter wire 300 nm. Arrays 6.5*3.2 μm^2	~10-20 pW/ wire	100-200	0.02		16

TABLE 2
TESTS RESULTS SIMULATING BURIED PIEZOELECTRIC CABLE UNDER CONTINOUS ROAD TRAFFIC

β (°)	Test N.	Δτ (s)	ΔT (s)	n_o (rpm)	v (km/h)	Peak voltage(mV)
22	1	0.156	1.284	23.364	60.923	538.531
	2	0.136	1.148	26.132	69.882	531.581
	3	0.120	1.000	30.000	79.200	643.253
	4	0.108	0.892	33.632	88.000	647.536
	5	0.096	0.804	37.313	99.000	779.142
	6	0.088	0.736	40.761	108.000	821.405
	7	0.082	0.674	44.510	115.902	794.013
45	8	0.332	1.340	23.388	28.627	476.660
	9	0.284	1.148	26.132	33.465	454.793
	10	0.248	1.000	30.000	38.322	549.714
	11	0.220	0.892	33.632	43.200	601.004
	12	0.196	0.800	37.500	48.490	723.335
	13	0.178	0.734	40.872	53.393	818.550
	14	0.168	0.674	44.510	56.571	900.096
90	15	0.680	1.360	22.059	13.976	551.763
	16	0.576	1.156	25.952	16.500	675.318
	17	0.500	1.004	29.880	19.008	743.948
	18	0.444	0.888	33.784	21.405	770.583
	19	0.404	0.806	37.221	23.525	818.952
	20	0.368	0.732	40.984	25.826	886.554

	21	0.340	0.676	44.379	27.953	847.158

The test bench is composed by a computer controlled rotating platform droved by a geared ac-motor. The angle between its axes (β)(°) (each axis comprises a pair of wheels) and the selection of the rotating angular speed (n_o)(rpm), see (1), simulates the time between the pass of the two axes (Δτ)(s) of a real vehicle.

$$\Delta\tau = \frac{\beta}{n_o \cdot 6} \quad (1)$$

The equivalent speed of a vehicle having a well known distance between its front and rear axis (b)(m) (in table 2 it's used a distance of b= 2,64 m, that is a common distance in sedan type cars) is calculated using (2).

$$v = \frac{b}{\Delta\tau \cdot 100} \cdot 3{,}6 \quad (2)$$

Fig. 3 describes the electrical results obtained in the 14th test of table 2, acquired with an Agilent Technologies TDS7054 scope, test probe 10073C (10:1, 500 MHz BW) and 1 MΩ as selected input impedance.

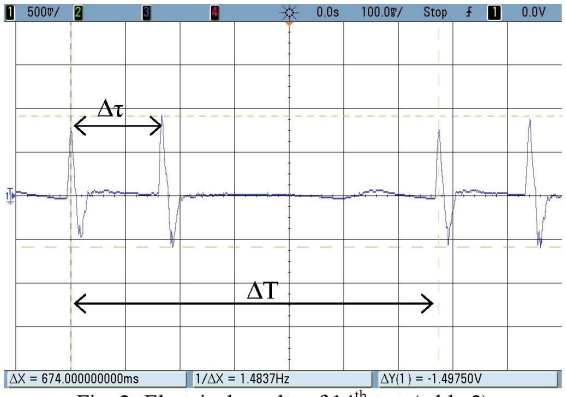

Fig. 3: Electrical results of 14th test (table 2)

2.2 Electrical Equivalent Models

The experimental results in our laboratory simulate the behavior of buried piezoelectric cables in real traffic sensing applications. The electrical model [23, 24] of the piezoelectric element excited by the mechanical action of the road traffic is composed by the Thèvenin association of the voltage generator in series with the capacitance of the piezoelectric cable or by the Norton equivalent, formed by a current generator associated in parallel with that capacitance.

We assume that the periodical mechanical excitation provided by the test bench is equivalent to continuous real traffic. The periodical nature of the electrical signals collected justifies the use of the Fourier mathematical analysis exposed in our method. The method is resumed in five steps.

- Extract the amplitude and time values of each test, for one electrical period of the signal (ΔT)(s), to write a text file with that values.
- Calculate the Fourier components of that signal, until the necessary harmonic. We use the well known electronic simulator PSpice, and its voltage generator VPWL_F_RE_FOREVER with the above text file.
- Test the simulation results of the series association of the harmonic components and the original signal of the text file with a load resistance in both cases approaching open load (1000GΩ).
- Apply the superposition principle and calculate the inner generators that in series with the capacitance of the piezoelectric material perform the real model of the piezoelectric element.
- Test the above electric real model with a 1 MΩ load resistor, equivalent to the probe impedance that has been used to obtain the electrical initial measurements.

The number of equivalent Fourier components in series with the equivalent capacitance of the material is between 75 and 100, using the total number of decimal positions to avoid the electric noise produced if the number of decimals were truncated.

In Fig. 4 is presented the equivalent 75 generators of the real model of the test 14th (table 2), see Fig. 3.

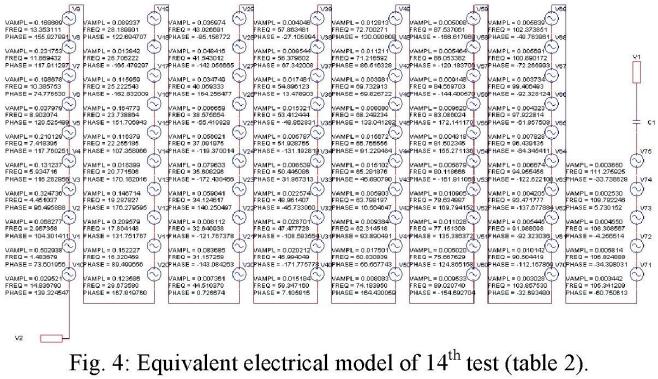

Fig. 4: Equivalent electrical model of 14th test (table 2).

It is presented the amplitude, phase and frequency values of every Fourier component of that model.

Finally, in Fig. 5 is represented the comparison of the last step of the method. The error is less than 2%, so we can evaluate the performance of piezoelectric materials (not only piezoelectric cables) in power harvesting related to road traffic environment.

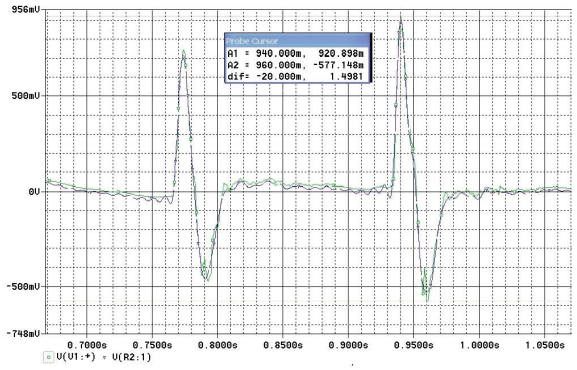

Fig. 5: Model 14th (table II) validated

3 Energy Harvesting using the Models

The generators modeled are in correspondence with consecutives buried piezoelectric cables. The practical distance of 1,6 cm between them was obtained by experimental results. This new parameter is included in the models as a time delay between the generators associated to consecutive cables using (3).

$$t_D = \frac{d_c}{n_o \cdot \left(\Pi/30\right) \cdot R} \quad (3)$$

In (3) t_D is expressed in seconds, d_c (m), n_o (rpm), and R (m) is the rotating platform radio of the test bench. As R=0,75m>>d_c=0,016m, we are using the geometric approximation between arc and chord.

The value of the capacitor used to hold the charge from the piezoelectric cables, is set constant in order to compare the results. Its value will affect the time needed to achieve the steady state. To collect charge from the positive and negative stress, semiconductor topologies are used. Its type and optimized structure is presented in the next item.

3.1 Rectifier Topologies

In this section the compared results of several rectifying structures and the influence of the semiconductor diode type is presented. In the first analysis, the values of the capacitor and the load resistor were constant.

The association of generators (one from one individual piezoelectric cable) was studied using bridge rectifiers connected in parallel or using polyphasic structures, i.e. star topology. The polyphasic topology in D structure was very soon rejected by its poor results.

We present in Fig. 6 (a) an example of 16 cables (having internal structure like Fig. 4) associated by rectifier bridges in parallel. This is the inner structure of one hierarchical block, and these hierarchical blocks are associated in parallel in order to perform a great number of cells in parallel, Fig. 6 (b).

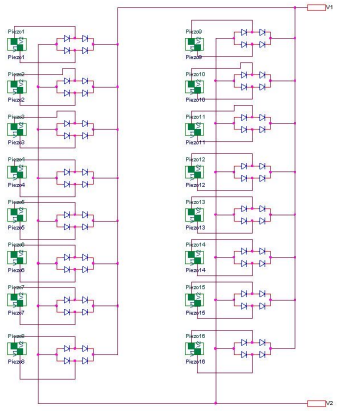

(a)

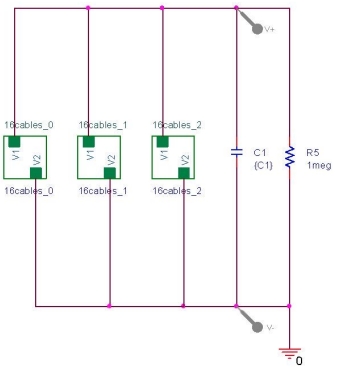

(b)

Fig. 6: (a) Bridge rectifiers in parallel association (b) 48 bridge rectifiers in parallel formed by 3 hierarchical blocks like 6(a).

Fig. 7 resumes the results of 48 piezoelectric generator cables associated using silicon rectifier diodes (1N400X type), Schottky diodes (BAS40-04W and RB751 type) and signal diodes (1N4148 type) used in the topological rectifier structures analyzed. The simulation time in computers Intel® Core™ 2 E8400 @ 3 GHz, 2 GB RAM, was 26 hours if Schottky diodes were used and 16 hours if 1N4148 diodes were used. All the studies executed later were performed with 1N4148 diodes.

Fig. 8 presents the maximum output voltage reached of 1,033.80 mV, using 80 models of piezoelectric generators associated in parallel with

1N4148 bridges. On next section we present results using series association of paralleled structures and mechanical amplification simulating heavy traffic.

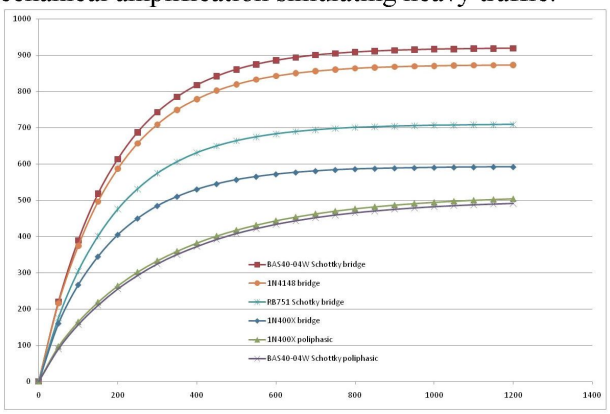

Fig. 7: Output voltage (mV) vs. time (s)

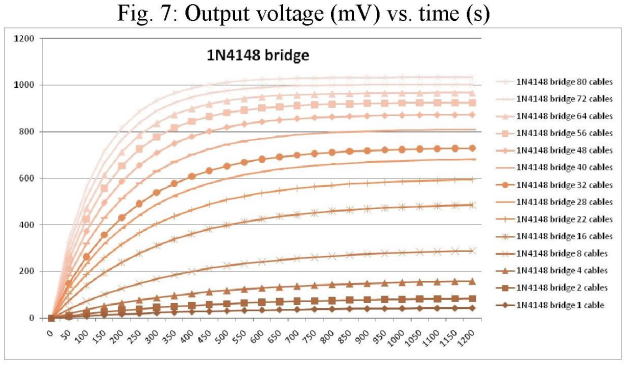

Fig. 8: 1N4148 bridge: Output voltage (mV) vs. time (s)

3.2 Final Results

The results of the harvester formed by the series association of two 80 parallel circuits, using a set of resistor values from open load to 100 Ω, are depicted in Fig. 9. The 160 GB data file obtained with each one of the load conditions made impossible use the PSpice parametric study because the hard disk capacity.

In Fig. 9(b), it's presented the relation between power vs. current supplied to the load resistor. The point of maximum value verifies (4).

$$P_{RoutMÁX} = \frac{V^2_{oc}}{4 \cdot R_o} \quad (4)$$

This applies when the value of load resistor equals the output equivalent resistance (R_o) of the harvesting circuit. The high value found of R_o and the open load voltage (V_{oc}), limits the practical power to be harvested. Table 3 presents maximum power and the parameters of the lineal input stage final model, including results for the test with mechanical amplification, which simulates the effect of heavy traffic. Their graphical results are presented in Fig. 9 (c) and (d). At the optimal point of operation, mechanical amplification has an incremental voltage factor of 4,27 over the results without it, so the ratio for power collected is about $(4,27)^2 = 18,28$.

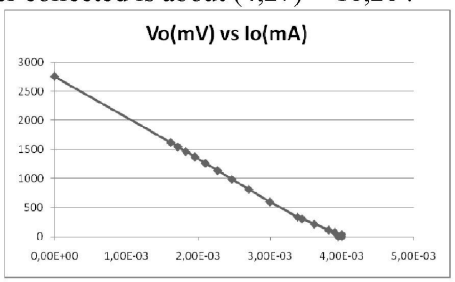

(a)

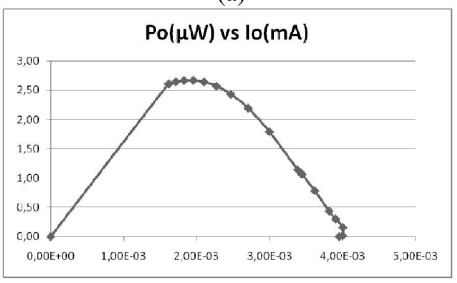

(b)

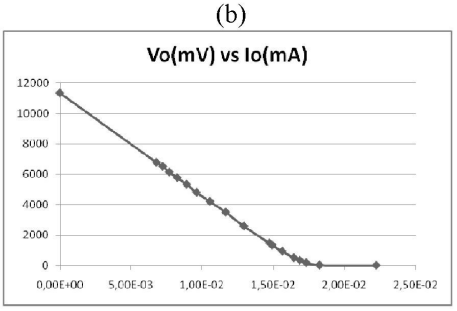

(c)

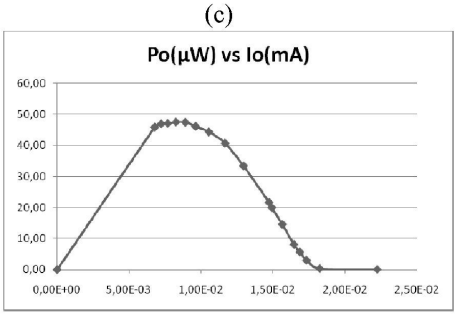

(d)

Fig. 9: Final results. Model without mechanical amplification (a), (b).Model with mechanical amplification (c), (d)

TABLE 3
EQUIVALENT FINAL LINEAL MODEL: PARAMETERS AND MAXIMUM OPTIMAL POWER.

TEST using mechanical amplification	V_{oc} (mV)	R_o (Ω)	$P_{RoutMÁX}$ (µW)
NO	2,748.3	715,431	2.635
YES	11,341	666,300	48.258

4 Conclusion

The methodology to obtain generalized electrical

equivalent models of piezoelectric materials specifically designed to be involved under road traffic mechanical stimulus, is presented.

The analysis of the optimal input stage of an energy harvesting system using piezoelectric materials, and its linearized electrical model are also covered. The equivalent model should be used in the design process of the following regulator circuit.

The optimal harvested power results shown, with mechanical amplification, guarantees the availability of self-powering a practical sensor's network, in civil and road applications, if the piezoelectric devices have enough mechanical amplification in locations with no power lines available.

Acknowledgement:

This work was supported in part by the project MAT2010-21088-C03-03

References:

[1] K. A. Cook-Chennault, N. Thambi, & A. M. Sastry, Powering MEMS portable devices—A review of nonregenerative and regenerative power supply systems with special emphasis on piezoelectric energy harvesting systems. *Smart Mat. & Struc.*,17,2008,33p.

[2] K. A. Cook-Chennault; N. Thambi; M.A. Bitetto; E.B. Hameyie, Piezoelectric Energy Harvesting: A Green and Clean Alternative for Sustained Power Production, *Bulletin of Science, Technology & Society*, vol. 28, 6, 2008, pp. 496-509.

[3] S. Priya, C.T. Chen, D. Fye & J. Zahnd, Piezoelectric windmill: A novel solution to remote sensing. *Jap. Journal of Appl. Physics: Part 2—Letters & Express Letters*, 44 (1-7), 2005, L104-L107.

[4] N. S. Shenck & J. A. Paradiso, Energy scavenging with shoe-mounted piezoelectrics. *IEEE Micro*, 21 (3), 2001, pp. 30-42.

[5] V. H. Schmidt, Piezoelectric energy conversion in windmills. *IEEE Ultrasonic Symp.*, 1992, pp. 897-904.

[6] M. J. Ramsay & W. W. Clark, Piezoelectric energy harvesting for bio MEMS applications. *Smart Struct. and Materials, Ind. Proc. of SPIE*. 2001,pp. 429-438.

[7] S. R. Platt, S. Farritor, K. Garvin & H. Haider, The use of piezoelectric ceramics for electric power generation within orthopedic implants. *IEEE-ASME Trans. on Mechatronics*, 10 (4), 2005, pp 455-461.

[8] Y. B. Jeon, R. Sood, J. H. Jeong, S. G. Kim, MEMS power generator with transverse mode thin film PZT, *Sens. and Act. A: Physical*, 122(1), 2005, pp16-22.

[9] N. M. White, P. Glynne-Jones & S. P. Beeby, A novel thick-film piezoelectric micro-generator. *Smart Materials & Structures*, 10 (4), 2001, pp. 850-852.

[10] S. Roundy & P. K. Wright, A piezoelectric vibration based generator for wireless electronics. *Smart Materials & Structures*, 13 (5), 2004, pp 1131-1142.

[11] S. Whalen, M. Thompson, D. Bahr, C. Richards & R. Richards, Design, fabrication and testing of the P 3 micro heat engine. *Sensors. and Actuators A: Physical*, 104 (3), 2003, pp. 290-298.

[12] H. W. Kim, A. Batra, S. Priya, K. Uchino, D. Markley, R. E. Newnham, H. F. Hofmann, Energy harvesting using a piezoelectric "cymbal" transducer in dynamic environment. *Jap. Jour. Appl. Phys.* 43, 2004, pp 6178-6183.

[13] T. G. Engel, C. Keawboonchuay & W. C. Nunnally, Energy conversion and high power pulse production using miniature piezoelectric compressors, *IEEE Trans. on Plasma Science*, 28 (5), 2000, pp. 1338-1341.

[14] K. L. Ren, Y. M. Liu, X. Geng, H. F. Hofmann & Q. M. Zhang, Single crystal PMN-PT/epoxy 1-3 composite for energy harvesting application. *IEEE Trans. on Ultrasonics, Ferroelectrics, and Frequency Control*, 53 (3), 2006, pp. 631-638.

[15] Sheng Wang, Kwok Ho Lam, Cheng Liang Sun, Kin Wing Kwok, Helen Lai Wa Chan, Ming Sen Guo and Xing-Zhong Zhao, Energy harvesting with piezoelectric drum transducer, *Appl. Phys. Lett.* 90, 113506, 2007.

[16] Zhong Lin Wang, Jinhui Song, Piezoelectric Nanogenerators Based on Zinc Oxide Nanowire Arrays, *Sience* Vol. 312 no. 5771, 2006, pp. 242-246.

[17] Chung-Bang Yun and Jiyoung Min, Smart Sensing, Monitoring, and Damage Detection for Civil Infrastructures, *KSCE Journal of Civil Engineering* 15(1), 2011, pp.1-14.

[18] N. Elvin, A. Elvin, D.H. Choi, A self-powered damage detection sensor, *J. Strain Anal.*,38(2), 2003, pp.115–124.

[19] M. Vázquez Rodríguez, F.J. Jiménez Martínez, J. de Frutos. Banco de ensayos para materiales piezoeléctricos en aplicaciones viales. *Bol. Soc. Esp. Ceram. Vidr.* Vol 50. 2, 2011, pp. 65-72.

[20] M. Zhu, E. Worthington, J. Njuguna, Analyses of power output of piezoelectric energy-harvesting devices directly connected to a load resistor using a coupled piezoelectric-circuit finite element method, *IEEE Trans. Ultrason. Ferroelectr. Freq. Control* 56, 2009, pp. 1309–1317.

[21] J. Sun, D. M. Mitchell, M. F. Greuel, R. M. Bass, Averaged modeling of PWM converters in discontinuous conduction mode, *IEEE Trans. Power Electron.*, vol. 16, 2001, pp. 482–492.

[22] G. K. Ottman, A. C. Bhatt, H. Hofmann, G. A. Lesieutre, Adaptive piezoelectric energy harvesting circuit for wireless remote power supply, *IEEE Trans. Power Electron.*, vol. 17, 2002, pp. 669–676.

[23] G.K. Ottman, H.F. Hofmann, G.A. Lesieutre. Optimized piezoelectric energy harvesting circuit using step-down converter in discontinuous conduction mode, *IEEE Trans. Power Elec.* 18 (2), 2003, pp. 696–703.